Preprints.org

Article

Not peer-reviewed version

Preparation of green brucite [NixMg1-x(OH2)] resulting from the combination of nickel ions and periclase (MgO) applied against yeast and bacteria

Cassio Siqueira , Aline B. Schons , Patrícia Appelt , Weslei D. Silva , Nayara Balaba , Mário A. A. Da Cunha , Fauze J. Anaissi *

Posted Date: 7 September 2023

doi: 10.20944/preprints202309.0442.v1

Keywords: periclase; green brucite; biocide; microbiology

Preprints.org is a free multidiscipline platform providing preprint service that is dedicated to making early versions of research outputs permanently available and citable. Preprints posted at Preprints.org appear in Web of Science, Crossref, Google Scholar, Scilit, Europe PMC.

Copyright: This is an open access article distributed under the Creative Commons Attribution License which permits unrestricted use, distribution, and reproduction in any medium, provided the original work is properly cited.

Preprints (www.preprints.org) | NOT PEER-REVIEWED | Posted: 7 September 2023 doi:10.20944/preprints202309.0442.v1

Disclaimer/Publisher's Note: The statements, opinions, and data contained in all publications are solely those of the individual author(s) and contributor(s) and not of MDPI and/or the editor(s). MDPI and/or the editor(s) disclaim responsibility for any injury to people or property resulting from any ideas, methods, instructions, or products referred to in the content.

Article

Preparation of Green Brucite [$Ni_xMg_{1-x}(OH2)$] Resulting from the Combination of Nickel Ions and Periclase (MgO) Applied against Yeast and Bacteria

Cássio Siqueira [1], Aline B. Schons [1], Patricia Appelt [1], Weslei D. Silva [2], Nayara Balaba [1], Mário A. A. Cunha [2] and Fauze J. Anaissi [1,*]

[1] Department of Chemistry, Universidade Estadual do Centro-Oeste, UNICENTRO, Alameda Elio Antonio Dalla Vecchia, 838, 85040-167, Guarapuava, PR, Brazil; cassiosiqueira19@gmail.com (C. S); aleschons239@hotmail.com (A. B. S); nayarabalaba20@gmail.br (N. B); patriciaappelt@unicentro.br (P. A); anaissi@unicentro.br (F. J. A)

[2] Department of Chemistry, Universidade Tecnológica Federal do Paraná, UTFPR, Via do Conhecimento, KM 01, Pato Branco, PR, Brazil; wesleisilva@alunos.utfpr.edu.br (W. D. S.); mcunha@utfpr.edu.br (M. A. A)

* Correspondence: anaissi@unicentro.br

Abstract: Magnesium oxide is typically white and can be colorized with transition metal insertion by doping or by adsorption. We present the preparation of green colored hydroxide by the adsorption of nickel ions by porous MgO. MgO was prepared by the colloidal starch suspension method and used to remove nickel ions from the aqueous solution. The oxides and hydroxides, before and after adsorption, were characterized by X-ray diffraction technical, and show that a phase change occurs, a transition from periclase (MgO) to brucite (Mg(OH)2) due to the interaction with nickel salts (acetate, chloride, and nitrate). The FTIR spectrum corroborates with the DRX data on the formation of brucite like crystal lattices. The new samples present a green color, indicative of the incorpo-ration of the Ni2+ ions. Mixed oxides in the form of brucite were used in microbiological tests and showed action against fungi and bacteria, with bactericidal, bacteriostatic, or fungistatic function. Green brucite (NixMg1-x(OH)2) can be used as an inorganic pigment in white or colorless paints with a special biocidal property.

Keywords: periclase**;** green brucite; biocide; microbiology

1. Introduction

Usually in the field of inorganic pigments metal oxides are closely attached to the subject, may it be by researching to synthetize new pigments by combination of chromo-phore, usually metals, with diverse support structures, example metal oxides, new syn-thetic routes, or optimization of already know pigments properties [1,2].

Recently the compound MgO have attracted great attention of scientists for his properties of diverse nanostructures, high surface area and nontoxicity [3]. Thus, a vast number of applications are being explored on different fields such as catalysis [4], superconductor [5], biological activities [6–8], treatment of wastewater [9], pigments [3] and others more. One of the common ways of obtaining MgO is related to $Mg(OH)_2$ calcination [10]. It is related on literature that MgO and $Mg(OH)_2$ are interchangeable depending on the procedure of hydration or dehydration [11].

According to by Wang *et al*. [12] organic-inorganic pigments utilizing $Mg(OH)_2$ pigment for modifying polymer silane and afterward grafting on cellulose fiber were explored. The study also comments on the $Mg(OH)_2$ characteristics as flame retardant, low toxicity and cost, and smoke suppressing ability. In the work at Primo *et al.* [13] reported the search for new eco-friendly routes to synthetize zinc oxides as being related with the use of natural additives for their capabilities in reducing calcination temperature and complexing gelling. A natural additive utilized on the route was cassava starch, a biodegradable polysaccharide from renewable raw material sources, consisting of amylose and amylopectin molecules that are composed of D-glucose units [14].

© 2023 by the author(s). Distributed under a Creative Commons CC BY license.

Preprints (www.preprints.org) | NOT PEER-REVIEWED | Posted: 7 September 2023 doi:10.20944/preprints202309.0442.v1

Green is usually associated with nickel on octahedral sites as explained by Hajjajji *et al.* [15] when studying the synthesis of green olivine pigment ($NiSiO_4$) utilizing industry waste. Lately, the inorganic pigment academia field are researching NIR reflective pigments for their cooling abilities, and applications focus on roof paint [16,17]. Zou *et al.* [18] explain the influence of high nickel concentration may result in to increase of absorbance at NIR, which is not favorable for cooling action, nevertheless, nickel is a low-cost metal used as chromophore. Thus, doping $BaTi_5O_{11}$ with <10% concentration of nickel and the results obtained displayed high NIR reflection.

Hence, nickel is a metal chromophore utilized on the production of diverse inorganic pigments, and MgO properties form a promisor supporting structure, and up to this date no $NiMg(OH)_2$ applications as a pigment were found on literature. Therefore, the objective of the paper is to synthesize $NiMg(OH)_2$ green pigments and characterize these compounds evaluating the influence of precursor salt anion.

2. Materials and Methods

2.1. Synthesis of MgO from cassava starch

The utilized MgO was synthesized by the same route of Balaba *et al.* [19], using cassava starch. Where the experimental procedure began with the extraction of starch (500 g) in 2.5 L of deionized water under agitation for 3 h followed by sieving. Then the synthesized starch (300 g) was added to a becker together with magnesium nitrate (64 g) and left to react for 20 min under agitation. This mixture was calcinated at 750 °C for 1 h with a heating ramp of 10 min^{-1}. The white solid was pulverized using a pestle and mortar, and identified as MgO_{starch} or MgO_{st}.

2.2. Synthesis of $Ni_xMg_{1-x}(OH)_2$ pigments

The pigments were produced by combining the MgO_{st} and nickel salts, being them nickel acetate tetrahydrate [$Ni(C_2H_3O_2)_2.4H_2O$), P.A., Neon]; nickel chloride hexahydrate [$Ni(Cl)_2.6H_2O$), P.A., Neon]; nickel nitrate hexahydrate [$Ni(NO_3)_2.6H_2O$), P.A., Neon]. The reaction medium was 60 mL of deionized water where blended MgO (1 g) and the respective nickel salt (10 ml, 0.5 M, stock solution) and thus agitated by magnetic stirrer bar for 30 min. Afterward, the precipitate was retrieved from the medium by centrifugation and washed with deionized water, and left to dry in a desiccator. The last step was the sieving of the powder in 250 mesh. The samples were named Ni_{Ac} in reference to the acetate; Ni_{Cl} for chloride; and Ni_{NO3} for nitrate.

2.3. Characterization of compounds

The elemental composition of the structured MgOst and after adsorption of nickel were evaluated using an energy-dispersive X-ray spectrometer (EDX) (Shimadzu, Kyoto, Japan), model EDX-7000, containing an Rh tube, operating at 50 and 15 W. The crystalline structure and phase were characterized by X-ray diffractometry (XRD-D2 Phaser; Bruker, Billerica, MA, USA), with a copper cathode (λ = 1.5418 Å), 30 kV potential, 10 mA current, ranging between 10° and 80° (2θ) and with 0.2 °/s increments.), the crystallographic charts used were from International Centre of Diffraction Data (ICDD). The morphology of the MgOst particulate and the samples after adsorption was examined with a scanning electron microscope (SEM - Hitachi TM 3000 XSTEAM2) with accelerating voltage 15 kV. Fourier transform infrared spectroscopy was performed in a Perkin Elmer Frontier device (Waltham, MA, USA). The samples were analyzed from Attenuated Total Reflectance (ATR) mode. The colorimetric analysis was performed on the MgOst and the green pig-ments in the form of powder, and after application on the colorless paint, a portable col-orimeter (3nh, model NR60CP) with a D65 light source. The data representative of colori-metric (CIEL*a*b*) analyses are: the L* parameter is the brightness and ranges from 0 to 100. The parameter a* represents the variation between red and green, where +a tends to red and −a* tends to green. The parameter b* is the variation between blue and yellow, where +b* tends to yellow and −b* tends to blue. The h* parameter refers

Preprints (www.preprints.org) | NOT PEER-REVIEWED | Posted: 7 September 2023 doi:10.20944/preprints202309.0442.v1

to the hue angle (tan−1 b*/a*). The value of C* is the chroma and represents the color saturation of the sam-ples [20].

2.4. Microbiological testing

2.4.1. Minimal Inhibitory Concentration (MIC)

The test was performed according to the Clinical and Laboratory Standards Institute (CLSI) standards [21,22], with the precursor salt magnesium oxide and the products obtained from the syntheses, nickel-doped magnesium oxide, having three different anions: acetate, chloride and nitrate. The strains tested were the yeast *Candida albicans* (ATCC 10231); and the bacteria *Staphylococcus aureus* (ATCC 25923); *Escherichia coli* (ATCC 25922) and *Salmonella gallinarum* (ATCC 9184).

The microorganisms were adjusted on the McFarland scale using the spectrophotometer at a wavelength of 625 nm at a concentration of 1.5 x 108 CFU mL^{-1} (McFarland scale). Stock solutions were prepared at a ratio of 1.25 $\mu g.\mu L^{-1}$ (m/V) of the compounds in 10% DMSO, a previously tested concentration that does not interfere with the cytotoxicity of the microorganisms. The procedure was carried out in duplicate with a 96-well plate, and the compounds were tested at concentrations from 0.625 to 0.0048 $\mu g.\mu L^{-1}$, by serial microdilution. The compounds were added (100 µL) in the specific culture medium for each microorganism, homogenized, then the inoculum (20 µL) was added, and the plate was incubated for 24 h at 37 °C (bacteria) and 48 h at 28 °C (yeast). The positive controls used were chloramphenicol (1.2 $mg.mL^{-1}$ for bacteria) and fluconazole (100 $mg.mL^{-1}$ for yeast); the negative controls were the solvent DMSO 10% and growth control, which is only the culture medium. After the incubation time, an alcoholic solution of the dye TTC (0.12% m/v - 2,3,5-triphenyltetrazolium chloride) was added to all wells, and the plates were incubated again for another two hours. The minimum inhibitory concentration (MIC) was read for each microorganism and compost tested.

2.4.2. Minimal Bactericidal or Fungicidal Concentration (MBC/MFC)

The test MBC or MFC, were performed after the MIC reading, following the procedure recommended by Clinical and Laboratory Standards Institute (CLSI)[21,22]. In this case, the wells that showed inhibition values in the MIC test were transferred to a Petri plate containing the corresponding culture medium (Mueller-Hinton agar for bacteria; Sabourand dextrose agar for yeasts). Then the plate was incubated for the time required for each microorganism, and after that, it was verified if there was growth or no growth of colonies, allowing us to characterize the compost as bacteriostatic/fungiostatic or bactericidal/fungicidal.

3. Results

3.1. Characterization

3.1.1. Chemical analysis of samples by EDXRF

The composition of the samples, with respect to the percentage of nickel, was estimated by chemical analysis by energy dispersive X-ray fluorescence, and the results are in Table 1. The results point to a gradual increase in the number of nickel ions incorporated by MgO, this fact being associated with the solubility of the precursor salts. According to Handbook [23], section 4 - Properties of the Elements and Inorganic Compounds; nickel(II) nitrate hexahydrate has a solubility of 99.2g/100 mL H_2O (number #1886); is more soluble than nickel(II) chloride hexahydrate that presents solubility of 67.5g/100 mL H_2O (#1874), and the latter is more soluble than nickel(II) acetate tetrahydrate that has solubility of 16g/100 mL H_2O (#1864).

Preprints (www.preprints.org) | NOT PEER-REVIEWED | Posted: 7 September 2023 doi:10.20944/preprints202309.0442.v1

Table 1. EDXRF element analysis.

Nickel precursor salt	Mg (%)	Ni (%)	Estimated composition
MgO_{st}	99.841	-	$[Mg_{0.99}O]$
Acetate	90.867	8.789	$[Ni_{0.087}Mg_{0.91}(OH)_2]_{ace}$
Chloride	90.784	9.050	$[Ni_{0.090}Mg_{0.91}(OH)_2]_{chl}$
Nitrate	90.342	9.437	$[Ni_{0.094}Mg_{0.90}(OH)_2]_{nit}$

The interaction of the periclase phase with nickel(II) ions results in the formation of the brucite phase (Eq. 1); whose estimated composition is presented in Table 1.

$$MgO\ (periclase\ phase) + Ni^{2+}_{(aq)} \rightarrow NixMg1\text{-}x(OH)_2\ (brucite\ phase) \quad (1)$$

3.1.2. Structural analysis by X-ray diffraction (XDR)

The structural analysis of the synthetized MgO (Figure 1) identifies the periclase phase of MgO (ICDD: 01-075-0447) characterized by its face-center cubic configuration and peaks (111), (200), (220), (311) and (222) [24,25].

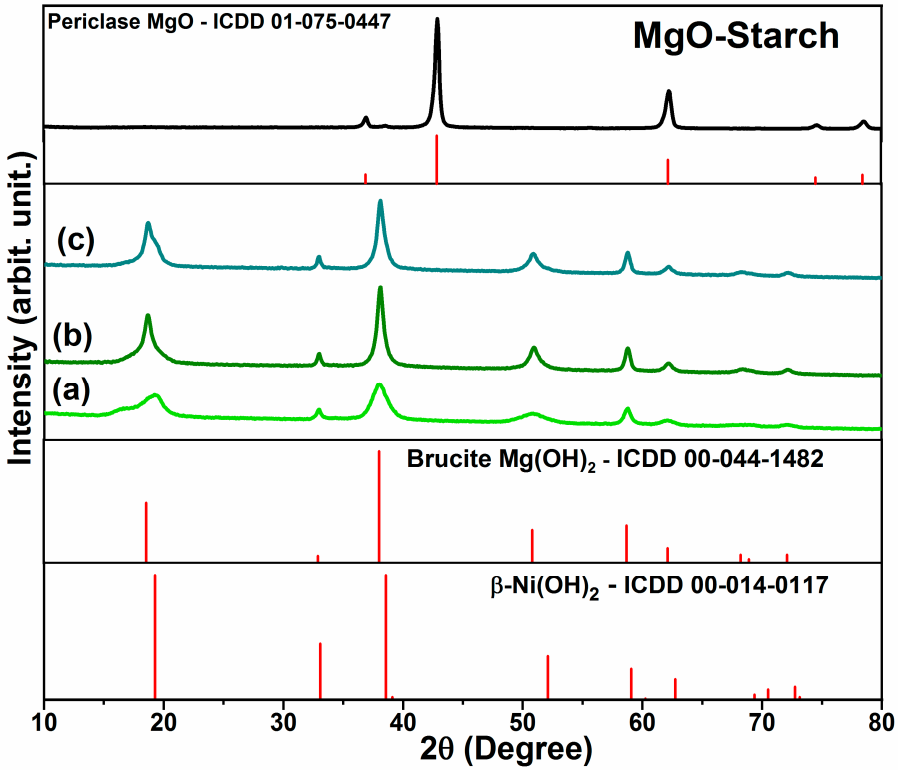

Figure 1. XDR of synthetized MgO, and $Ni_xMg_{1-x}(OH)_2$ the sequence order of precursor salt is (a) acetate (b) chloride (c) nitrate. Also were presented the XDR patterns of periclase, brucite and β-$Ni(OH)_2$ from the ICDD database.

As shown in Figure 1a–c, the identified peaks of $NixMg1\text{-}x(OH)_2$ compound X-ray diffractogram were (001), (100), (101), (102), (110), (111), (103), (200) and (201), being this crystalline phase determined as brucite, a hexagonal arrangement of $Mg(OH)_2$ (ICDD: 00-044-1482) [5,25,26]. Moreover, β-$Ni(OH)_2$ is isostructural to Mg(OH)2 with the brucite like crystal lattice [5,27].

3.1.3. Morphological characteristics by scanning electronic microscopy (SEM)

The morphological study of the piments is presented in Figure 2. It's possible to relate to literature already reported grain morphology configuration of $Mg(OH)_2$ [28]. Hence, on the Figure 2 (a-b) the acetate pigment presented less porous compared to the other precursor salts. Highlighting,

Preprints (www.preprints.org) | NOT PEER-REVIEWED | Posted: 7 September 2023 doi:10.20944/preprints202309.0442.v1

in Figure 2 (c2), the chloride compound presented this needle-like shapes that can be attributed to $Mg(OH)_2$ [29].

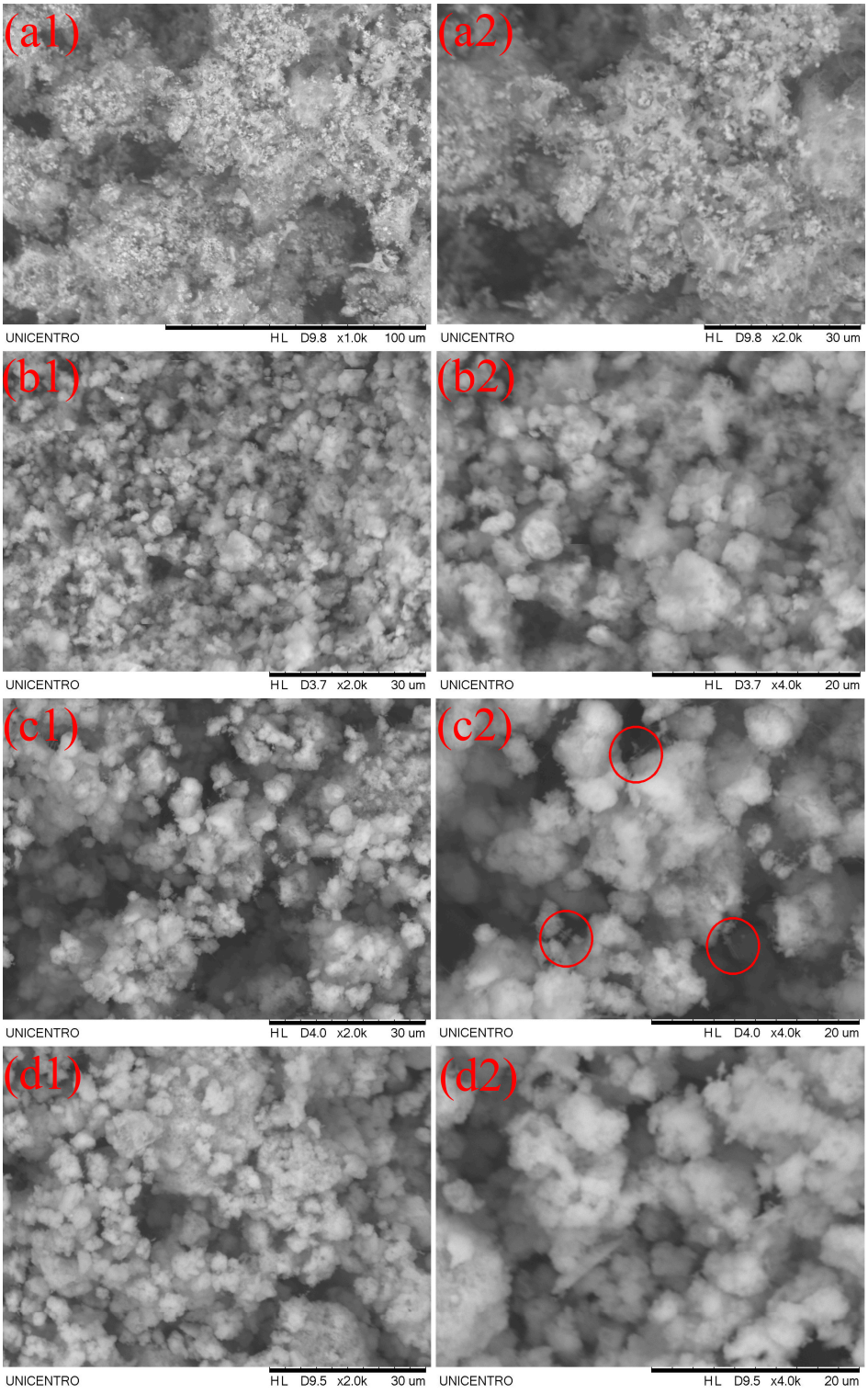

Figure 2. SEM imagens of pigments at 30 μm and 20 μm. (a) MgO_{st}; (b) Acetate; (c) chloride; (d) nitrate.

3.1.4. Fourier transform infrared spectroscopy (FTIR)

The infrared spectrum (Figure 3) identified the stretching of hydroxyl ν(OH) at 3691 cm^{-1} and the wide band 3358 cm^{-1} [25,27] for all compounds. The bands at spectrum (Figure 3a) at 1582 and 1398 cm^{-1} are from the symmetrical and asymmetrical $\nu(COO^-)$ [30,31]. Now in Spectrum (Figure 3b), bands at 1652 and 1443 cm-1 correspond to the ν(OH) of water molecule physiosorbed in the lattice

Preprints (www.preprints.org) | NOT PEER-REVIEWED | Posted: 7 September 2023 doi:10.20944/preprints202309.0442.v1

[6,25]. For the compound synthetized by nitrate the band of vibration modes of ν(NO3) interlayered are shown in the spectrum (Figure 3c), at 1384 cm^{-1}, and the other two bands at 1509 and 1323 cm^{-1} are associated to metal coordinated nitrate [31].

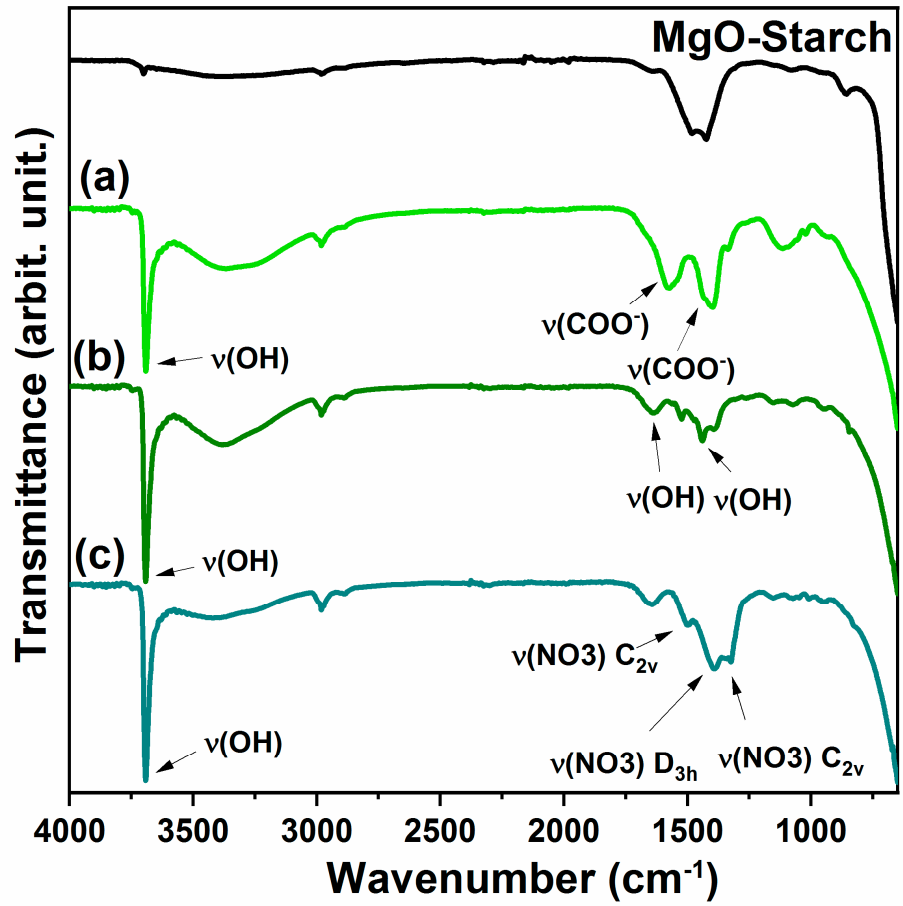

Figure 3. FTIR spectrum. (a) acetate (b) chloride (c) nitrate.

3.1.5. Colorimetric analysis and spectroscopy VIS-NIR

According to the absorbance electronic spectra in Figure 4a, the identified energy bands for the powder $Ni_xMg_{1-x}(OH)_2$ were at 678 nm and 745 nm. Also, reflectance bands Figure 4b are at 530 and 883 nm. Correlating the absorbance bands to the Laporte transitions from ground state [$^3A_{2g} \rightarrow {}^1E_g$] and [$^3A_{2g} \rightarrow {}^3T_{1g}(F)$] of nickel [15,32,33].

Preprints (www.preprints.org) | NOT PEER-REVIEWED | Posted: 7 September 2023 doi:10.20944/preprints202309.0442.v1

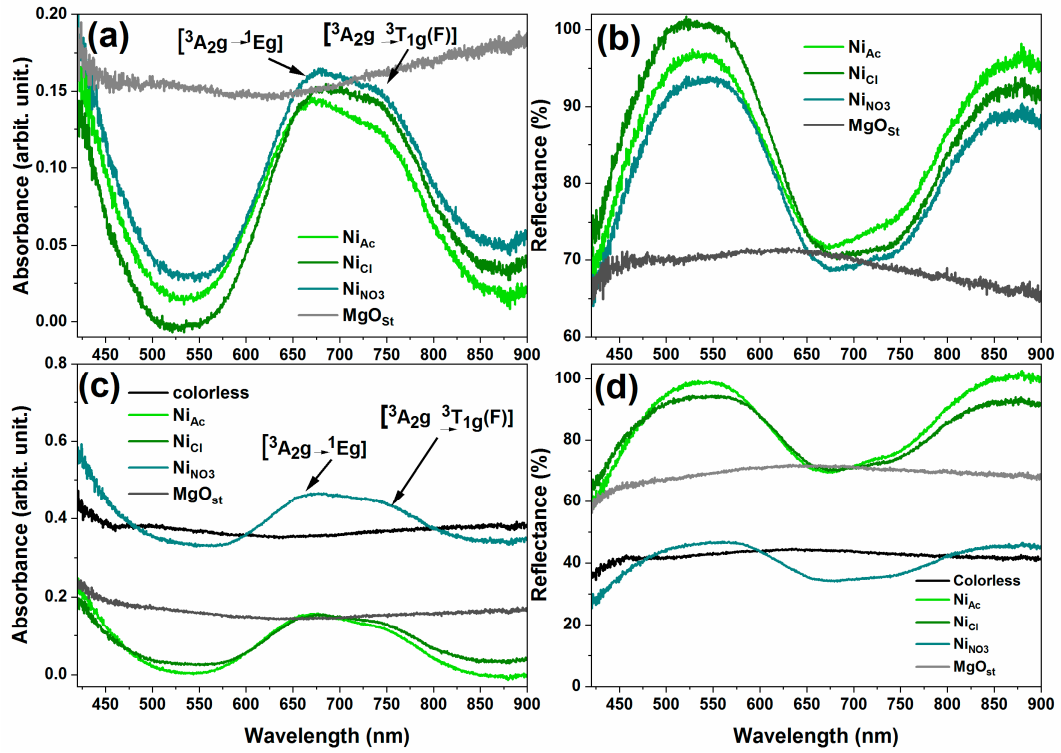

Figure 4. Electronic spectrum of absorbance and reflectance of solids. (a-b) powder pigments; (c-d) dispersed on colorless paint.

As a result of precursor salt on the reflectance Figure 4b the acetate displays less reflectance at band 530 nm but more intense band at 883 nm when compared to chlorine precursor pigment. The nitrate precursors demonstrated less band reflection intensity of the series.

The paint dispersed pigments electronic spectra as shown at Figure 4b,c present the same transitions as of the powder counterparts. The behavior of the pigment of nitrate as precursor convey more absorbance on the paint and consequently less reflectance. On the contrary, acetate and chloride increase the paint reflectance, being the acetate the more reflective in paint.

The colorimetric analysis utilizing CieL*a*b* color space is displayed in Table 2 for the powder pigments. From the data, it was observed that despite the different precursor salts, the samples did not show significant discrepancies between the Cie L*a*b* values. All the samples maintained the values in the quadrants green (-a*) and yellow (-b*). Similarly, there was no significant difference between the ΔE color difference values, which were ~ 17.

Table 2. Colorimetric analysis of powder pigments.

Sample	L*	a*	b*	C*	h*	ΔE	Software color
MgO	67.65	0.84	3.13	3.24	104.98	-	
Acetate	54.02	-8.56	7.61	11.45	138.34	17.15	
Chloride	54.28	-9.39	6.46	11.40	145.48	17.16	
Nitrate	54.35	-9.03	6.96	11.40	142.37	17.00	

Preprints (www.preprints.org) | NOT PEER-REVIEWED | Posted: 7 September 2023 doi:10.20944/preprints202309.0442.v1

For application as a microbiological action, the pigments were dispersed in colorless paint and applied to paper. The test specimens were also evaluated according to the Cie L*a*b* metrics (Table 3) and were also applied to plaster blocks (Table 4) for comparison purposes. After the dispersion, the L* values increased due to the interference of the color of the paper and plaster. For the pigments on paper, the discrepancy color was observed for the Chloride pigment (Nicl), the ΔE showed a lower value compared to the colorless paint. For the samples dispersed in colorless paint and in the blocks, the lowest color variation was for the Nitrate pigment with a value ~ 8.5.

Table 3. Colorimetric analysis of dispersed on paper with colorless paint pigments.

Sample	L*	a*	b*	C*	h*	ΔE	Software color
Colorless paint	65.04	-0.95	2.91	3.06	108.14	-	
MgO	78.49	0.54	4.42	4.45	96.90	13.62	
Acetate	70.60	-13.07	10.67	16.87	140.77	15.43	
Chloride	64.59	-9.20	7.64	11.96	140.31	9.52	
Nitrate	72.36	-12.22	11.13	16.53	137.68	15.75	

Table 4. Colorimetric analysis of dispersed on plaster block with colorless paint pigments.

Sample	L*	a*	b*	C*	h*	ΔE	Software color
Colorless paint	88.00	-0.06	4.37	4.37	90.34	-	
MgO	86.99	0.53	4.42	4.45	96.90	1.17	
Acetate	82.87	-7.48	10.65	13.01	125.07	11.00	
Chloride	83.46	-6.77	9.07	11.31	126.75	9.37	
Nitrate	85.49	-5.83	10.03	11.60	120.16	8.46	

The Figure 5, show the comparation between the powder pigments in relation the white pigment MgOst Thus, it is that acetate and chloride are approximate on the color space, differing for small a* and b* values, in contrast the nitrate varies great amount on the a* and b* by reducing these values, resulting in a less green and yellow pigment.

Preprints (www.preprints.org) | NOT PEER-REVIEWED | Posted: 7 September 2023 doi:10.20944/preprints202309.0442.v1

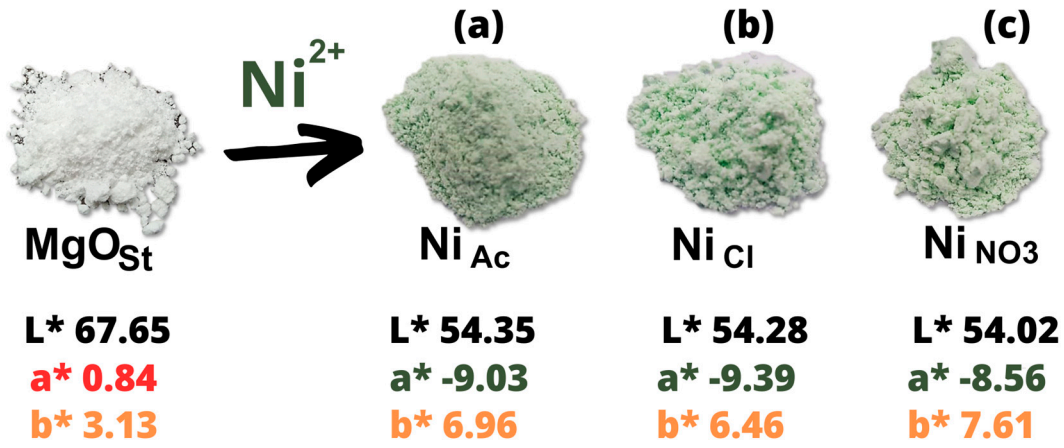

Figure 5. Cie L*a*b* space powder pigment, after and before adsorption nickel with salt of (a) acetate (Ni_{Ac}); (b) chloride; (Ni_{Cl}) and (c) nitrate (Ni_{NO3}).

3.2. Microbiological tests (MIC, MBC and MFC)

In general, the microbiological tests showed good results for the compounds; all oxides presented antimicrobial activity at the concentrations studied, showing that they can be used as antimicrobial agents.

According to Table 5, the same MIC value (0.625 $\mu g.\mu L^{-1}$) was found for Gram-positive strain of *S. aureus* and for Gram-negative strain of *S. gallinarum*, showing that the results encompassed a potential broad spectrum of activity.

For *E.coli*, the results were similar for the compounds MgO_{st}, Ni_{Ac} and Ni_{NO3}, exhibiting MIC equal to 0.625 $\mu g.\mu L^{-1}$. The compost Ni_{Cl} showed better activity, having a minimum inhibitory concentration of 0.312 $\mu g.\mu L^{-1}$, this can be explained by the difference in the chloride anion present in the structure of the compost, as already referenced in the literature [34,35].

Table 5. MIC test results for bacteria and yeast (in $\mu g.\mu L^{-1}$).

Sample	S. aureus	E. coli	S. gallinarum	C. albicans
MgO	0.625 (bc)	0.625 (bs)	0.625 (bs)	*
$Ni_xMg_{1-x}(OH)_2(Ac.)$	0.625 (bc)	0.625 (bs)	0.625 (bs)	0.625 (fs)
$Ni_xMg_{1-x}(OH)_2(Cl)$	0.625 (bc)	0.312 (bs)	0.625 (bs)	*
$Ni_xMg_{1-x}(OH)_2(NO_3)$	0.625 (bc)	0.625 (bs)	0.625 (bc)	0.625 (fs)

Legend: (bc) bactericidal, (bs) bacteriostatic, (fs) fungistatic. *Did not exhibit activity at the concentrations tested.

In the MBC assay for *S. aureus*, all compounds exhibited bactericidal potential at a concentration of 0.625 $\mu g.\mu L^{-1}$ (Table 4); however, for *E. coli*, all compounds were bacteriostatic at this same concentration, except for the compound Ni_{Cl}, which had bacteriostatic action at a concentration of 0.312 $\mu g.\mu L^{-1}$. For the bacteria *S. gallinarum* the compounds inhibited growth at the concentration of 0.625 $\mu g.\mu L^{-1}$ being bacteriostatic, except for Ni_{NO3} which had a bactericidal effect at the concentration cited.

For the yeast *Candida albicans*, the compounds containing acetate counter-ion Ni_{Ac} and nitrate Ni_{NO3} were the only ones in the series that inhibited the growth of the microorganisms at a concentration of 0.625 $\mu g.\mu L^{-1}$, respectively. However, in the MFC assay, colonies occurred after incubation, so they were considered fungistatic compounds.

It is noted that the compounds present better activity for bacteria than for the fungus tested. The bactericidal effect of the four compounds against the *S. aureus* strain stands out, highlighting greater inhibition against the Gram-positive strain. Among the compounds studied, Ni_{NO3} stands out, which showed activity against the four microorganisms studied, having biocide action against Gram-positive *S. aureus* and Gram-negative *S. gallinarum*, biostatic action on *E.coli* and also fungistatic action

Preprints (www.preprints.org) | NOT PEER-REVIEWED | Posted: 7 September 2023 doi:10.20944/preprints202309.0442.v1

against the yeast *C. albicans*, demonstrating the greatest inhibition potential among the four compounds tested.

4. Discussion

A simple route for the synthesis of green pigments from nickel and magnesium oxide based on solution-base hydroxide formation. As presented by the XRD, Figure 2, the structural crystalline phase identified was the brucite of $Mg(OH)_2$. Furthermore, β-$Ni(OH)_2$ is isostructural to $Mg(OH)_2$ [6,27]. The FTIR spectra (Figure 5), demonstrates that the compounds are a solid solution of $Ni_xMg_{1-x}(OH)_2$ because the band 3691 cm-1 is correlating to the metal-O less covalency interaction, compared to β-Ni(OH)2, in which directly influences the O-H bond, in way it becomes less polarized with more concentration of Mg in the lattice, shifting the ν(OH) band to higher wavenumbers [27]. Hence, the difference on electronegativity of Mg [1,2] and Ni [1,8] possibilities the exchange of Mg for Ni in the crystalline structure [27].

Brucite is the mineral form of magnesium hydroxide [$Mg(OH)_2$]. It is associated as a product of modification of the periclase phase found in marble [14]. Synthetic brucite is mainly used as a precursor to magnesia (MgO), an important refractory insulator [36]. It can be used as a flame retardant because it decomposes thermally and releases water in a similar way to aluminum hydroxide and mixtures of Huntite and Hydromagnesite.

The impact of the precursor salts on the characterization of the compounds were analyzes. The acetate anion influences the crystalline lattice, producing a more amorphous compound [26] as is document in literature for the β-$Ni(OH)_2$, and shown on the diffractogram Figure 2a, this being the resulting intercalation of the anion to the hexagonal structure [5,26]. Also is notable the appearance of the shoulder on peak at 2θ = 18° attributed to the shift on the (001) plane from the acetate intercalation [5,31]. Relating to the XRD data the FTIR bands, Figure 5a, at 1568 cm^{-1} and 1391 cm^{-1} identifying ν(COO^-) symmetric and asymmetric vibration modes [30,31], reinforcing the evidence of intercalation of the acetate anion on the structure. Synthesis utilizing nitrate nickel salt interfered as well on the crystallinity of the material, with the appearance of a shoulder on the 2θ = 18° peak, Figure 2c being this related to the presence of NO^{3-}, agreeing with the FTIR spectrum band of 1384 cm^{-1}, Figure 5c, that are typical of Dh3 symmetry of free NO^{3-} on the interlayer of the lamellar structure [31]. The chloride precursor produced the more crystalline compound when comparing the 100% peak at 2θ = 37° intensity and shape with the other precursors salts, Figure (b).

A morphological analysis, Figure 3, of the $Ni_xMg_{1-x}(OH)_2$ compounds exhibit the granular arrangement of $Mg(OH)_2$ [28]. Worth noting, the needle shape morphologies highlighted on Figure 4, for chloride precursor compound, can correlate to formation of 1D-like structure from the hexagonal configuration already discussed in literature [9,37] . Hao *et al.* [37] explains that the mechanism for formation of nanotubes follows the pathway of ionization of Mg to Mg^{+2}, and the results of utilizing NaCl as electrolyte offered more efficiency in the formation for said morphology when comparing to NaAc. Therefore, the exchange of Ni for Mg on the lattice of the structure allied with the anion chloride maybe the responsible for this morphology appearance.

After examining the electronic spectra, Figure X, we can now again relate to the structure of the pigments, as explained by Qi *et al.* [33] the brucite β-$Ni(OH)_2$ the optical properties are based on the metal d-d orbitals of nickel, considering that it is surrounded by six O in a typical octahedral configuration, endorsing the Ni exchange with Mg at the structure.

The color of the pigments was characterized utilizing the Cie L*a*b*. Subsequently, MgO is a white powder [38], the explanation is the Mg having no free electron to excite to 3s orbital after losing the two 3s electrons to form Mg-O bond, and the pigments present negative a*, at Cie L*a*b* color space this relates to intensity of green, thus confirming the Ni as the chromophore.

Regarding the application, some works, such as Balaba *et al.* (2023) [6], show that MgO has antimicrobial activity at a concentration of 400 $\mu g.mL^{-1}$ for *S. aureus*, E. coli and *C. albicans*; in comparison with this work, $Ni_xMg_{1-x}(OH)_2(Cl)$ stands out, which had an inhibition at a concentration of 0.312 $\mu g.\mu L^{-1}$, showing a better bacteriostatic action for Gram-negative bacteria. This is considered a good result because the inhibition of Gram-negative bacteria is more complex.

Preprints (www.preprints.org) | NOT PEER-REVIEWED | Posted: 7 September 2023 doi:10.20944/preprints202309.0442.v1

Studies such as Murtaza et al. (2023) [39] and Liao et al. (2023) [34] show that MgO has better efficiency when combined with other compounds and still has a wide range of applications, such as an alternative therapeutic approach or for the treatment of plants with bacterial infections. In the work of Nguyen et al. (2018) [41] on the study of the activity of the MgO compost, the inhibition activity was 1.0 mg.mL-1 for E. coli, 0.7 mg.mL-1 for S. aureus and 1.2 mg.mL-1 for C. albicans, respectively. When these values are compared with the data obtained in this work, it is observed that the MIC values were lower and that there is no need for such a high concentration to inhibit microbial growth, mainly considering that the doping with Ni and the anion of the compost interfere in the microbial inhibition activity, improving cytotoxic activity. For NPs (nanoparticles) of Ni(OH)2, the inhibition reaches 5 mg.ml-1, shown in the work of Chaudhari et al. (2022) [42].

5. Conclusions

The preparation of magnesium oxide by the colloidal starch suspension method leads to the formation of the periclase phase (MgO), a white oxide. When in contact with water, it undergoes self-hydrolysis and generates the brucite phase ($Mg(OH)_2$), with a tendency to remove metallic ions from wastewater. Each metal has a characteristic color, in the case of nickel ions the green color. In this way, the removal of metal ions results in inorganic pigments with special characteristics, in addition to color. Among the properties we can highlight the use as catalysts, photocatalysts, biocides, oxidizing or reducing agents, among others. Expanding the reuse of the product resulting from the treatment of water contaminated with metal ions.

Author Contributions: Conceptualization, C.S. and N.B.; methodology, C.S. and N.B.; validation, C.S.; N.B. and A.B.S.; formal analysis, C.S.; N.B. and A.B.S.; investigation, W.D.S; C.S. and A.B.S; resources, F.J.A.; writing—original draft preparation, C.S.; P.A. and A.B.S.; writing—review and editing, F.J.A. and M.A.A.C.; supervision, F.J.A. and P.A.; project administration, F.J.A.; funding acquisition, F.J.A. and M.A.A.C. All authors have read and agreed to the published version of the manuscript.

Funding: C.S. appreciates CNPq for an undergraduate scholarship (PIBIC). F.J.A. is thankful for a CNPq Productivity grant (310815/2022-3) and the grants CNPq (427127/2018-1).

Institutional Review Board Statement: Not applicable.

Informed Consent Statement: Not applicable.

Acknowledgments: The authors would like to thank the agencies for their support: Capes, CNPq, Finep, Fundação Araucária.

Conflicts of Interest: The authors declare no conflict of interest.

References

1. Monrós, G.; Llusar, M.; García, A.; Gargori, C.; Galindo, R. Development of New Ceramic Dyes.; October 27 2010; pp. 182–193.
2. Llusar, M.; Gargori, C.; Cerro, S.; Badenes, J.A.; Monrós, G. New Ceramic Pigments for the Coloration of Ceramic Glazes.; October 31 2014; pp. 148–158.
3. Pilarska, A.A.; Klapiszewski, Ł.; Jesionowski, T. Recent Development in the Synthesis, Modification and Application of Mg(OH)2 and MgO: A Review. *Powder Technol.* **2017**, *319*, 373–407, doi:10.1016/j.powtec.2017.07.009.
4. Ansari, A.; Ali, A.; Asif, M.; Shamsuzzaman, S. Microwave-Assisted MgO NP Catalyzed One-Pot Multicomponent Synthesis of Polysubstituted Steroidal Pyridines. *New J. Chem.* **2018**, *42*, 184–197, doi:10.1039/C7NJ03742B.
5. Yin, J.; Zhou, G.; Gao, X.; Chen, J.; Zhang, L.; Xu, J.; Zhao, P.; Gao, F. α- and β-Phase Ni-Mg Hydroxide for High Performance Hybrid Supercapacitors. *Nanomaterials* **2019**, *9*, 1686, doi:10.3390/nano9121686.
6. Balaba, N.; Jaerger, S.; Horsth, D.F.L.; Primo, J. de O.; Correa, J. de S.; Bittencourt, C.; Zanette, C.M.; Anaissi, F.J. Polysaccharides as Green Fuels for the Synthesis of MgO: Characterization and Evaluation of Antimicrobial Activities. *Molecules* **2023**, *28*, doi:10.3390/molecules28010142.
7. Tang, Z.-X.; Lv, B.-F. MgO Nanoparticles as Antibacterial Agent: Preparation and Activity. *Brazilian J. Chem. Eng.* **2014**, *31*, 591–601, doi:10.1590/0104-6632.20140313s00002813.
8. Ohira, T.; Yamamoto, O. Correlation between Antibacterial Activity and Crystallite Size on Ceramics. *Chem. Eng. Sci.* **2012**, *68*, 355–361, doi:10.1016/j.ces.2011.09.043.

Preprints (www.preprints.org) | NOT PEER-REVIEWED | Posted: 7 September 2023 doi:10.20944/preprints202309.0442.v1

9. Zhang, S.; Cheng, F.; Tao, Z.; Gao, F.; Chen, J. Removal of Nickel Ions from Wastewater by Mg(OH)2/MgO Nanostructures Embedded in Al2O3 Membranes. *J. Alloys Compd.* **2006**, *426*, 281–285, doi:10.1016/j.jallcom.2006.01.095.
10. Nobre, J.; Ahmed, H.; Bravo, M.; Evangelista, L.; de Brito, J. Magnesia (MgO) Production and Characterization, and Its Influence on the Performance of Cementitious Materials: A Review. *Materials (Basel).* **2020**, *13*, 4752, doi:10.3390/ma13214752.
11. Kumari, L.; Li, W.Z.; Vannoy, C.H.; Leblanc, R.M.; Wang, D.Z. Synthesis, Characterization and Optical Properties of Mg(OH)2 Micro-/Nanostructure and Its Conversion to MgO. *Ceram. Int.* **2009**, *35*, 3355–3364, doi:10.1016/j.ceramint.2009.05.035.
12. Wang, X.; Zhang, Y.; Lv, L.; Cui, Y.; Wei, C.; Pang, G. Preparation of Mg(OH)2 Hybrid Pigment by Direct Precipitation and Graft onto Cellulose Fiber via Surface-Initiated Atom Transfer Radical Polymerization. *Appl. Surf. Sci.* **2016**, *363*, 189–196, doi:10.1016/j.apsusc.2015.11.259.
13. Primo, J. de O.; Bittencourt, C.; Acosta, S.; Sierra-Castillo, A.; Colomer, J.F.; Jaerger, S.; Teixeira, V.C.; Anaissi, F.J. Synthesis of Zinc Oxide Nanoparticles by Ecofriendly Routes: Adsorbent for Copper Removal From Wastewater. *Front. Chem.* **2020**, *8*, 571790, doi:10.3389/FCHEM.2020.571790/BIBTEX.
14. Brito, G.F.; Agrawal, P.; Araújo, E.M.; Mélo, T.J.A. Biopolímeros, Polímeros Biodegradáveis e Polímeros Verdes. *Rev. Eletrônoca Mater. e Process.* **2011**, *6*, 127–139.
15. Hajjaji, W.; Costa, G.; Zanelli, C.; Ribeiro, M.J.; Seabra, M.P.; Dondi, M.; Labrincha, J.A. An Overview of Using Solid Wastes for Pigment Industry. *J. Eur. Ceram. Soc.* **2012**, *32*, 753–764, doi:10.1016/j.jeurceramsoc.2011.10.018.
16. Zou, J.; Chen, Y.; Zhang, P. Influence of Crystallite Size on Color Properties and NIR Reflectance of TiO2@NiTiO3 Inorganic Pigments. *Ceram. Int.* **2021**, *47*, 12661–12666, doi:10.1016/j.ceramint.2021.01.126.
17. Wei, X.; Zou, X.; Deng, Z.; Bao, W.; Ai, T.; Zhang, Q. Synthesis and Characterisation of Mg2+ and Al3+ Co-Doped CoCr2O4 Inorganic Pigments With High Near-Infrared Reflectance. *Front. Mater.* **2022**, *9*, doi:10.3389/fmats.2022.850115.
18. Zou, J.; Zhang, P. Ni-Doped BaTi5O11: New Brilliant Yellow Pigment with High NIR Reflectance as Solar Reflective Fillers. *Ceram. Int.* **2020**, *46*, 3490–3497, doi:10.1016/j.ceramint.2019.10.063.
19. Balaba, N.; Jaerger, S.; Horsth, D.F.L.; Primo, J. de O.; Correa, J. de S.; Bittencourt, C.; Zanette, C.M.; Anaissi, F.J. Polysaccharides as Green Fuels for the Synthesis of MgO: Characterization and Evaluation of Antimicrobial Activities. *Molecules* **2022**, *28*, 142, doi:10.3390/molecules28010142.
20. Bible, B.B.; Singha, S. Canopy Position Influences CIELAB Coordinates of Peach Color. *Hortscience* **1993**, *28*, 992–993, doi:10.21273/HORTSCI.28.10.992.
21. Clinical and Laboratory Standarts Institute (CLSI) *Reference Method for Broth Dilution Antifungal Susceptibility Testing of Yeasts;* Third edit.; Wayne, Pa, USA, 2008; ISBN 610.688.0700.
22. Clinical and Laboratory Standarts Institute (CLSI) *Methods for Dilution Antimicrobial Susceptibility Tests for Bacteria That Grow Aerobically*; Sixty Edit.; . NCCLS document M7-A6, Suite 1400, Wayne, Pennsylvania, USA, 2003; ISBN 610.688.0700.
23. Haynes, W.M.; Lide, D.R.; Bruno, T.L. *CRC Handbook of Chemistry and Physics*; 95th ed.; Taylor & Francis Group, 2014; ISBN 978-1-4822-0868-9.
24. Vinokurov, S.E.; Kulikova, S.A.; Krupskaya, V. V.; Tyupina, E.A. Effect of Characteristics of Magnesium Oxide Powder on Composition and Strength of Magnesium Potassium Phosphate Compound for Solidifying Radioactive Waste. *Russ. J. Appl. Chem.* **2019**, *92*, 490–497, doi:10.1134/S1070427219040049.
25. Yousefi, S.; Ghasemi, B.; Nikolova, M.P. Opto-Structural Characterization of Mg(OH)2 and MgO Nanostructures Synthesized through a Template-Free Sonochemical Method. *Appl. Phys. A* **2021**, *127*, 549, doi:10.1007/s00339-021-04605-7.
26. Kovalenko, V.; Kotok, V. Synthesis of Nickel Hydroxide in the Presence of Acetate Ion as a «soft» Ligand for Application in Chemical Power Sources. *Eastern-European J. Enterp. Technol.* **2019**, *6*, 6–12, doi:10.15587/1729-4061.2019.185313.
27. de Oliveira, E.F.; Hase, Y. Infrared Study of Magnesium–Nickel Hydroxide Solid Solutions. *Vib. Spectrosc.* **2003**, *31*, 19–24, doi:10.1016/S0924-2031(02)00049-8.
28. Prorok, R.; Ramult, J.; Nocun-Wczelik, W.; Madej, D. The Effect of Chelate Compounds on the Hydration Process of MgO–Al2O3 Phase System under Hydrothermal Conditions. *Appl. Sci.* **2021**, *11*, 2834, doi:10.3390/app11062834.
29. Yousefi, S.; Ghasemi, B.; Tajally, M.; Asghari, A. Optical Properties of MgO and Mg(OH) 2 Nanostructures Synthesized by a Chemical Precipitation Method Using Impure Brine. *J. Alloys Compd.* **2017**, *711*, 521–529, doi:10.1016/j.jallcom.2017.04.036.
30. Sajilal, K.; Moses Ezhil Raj, A. Effect of Thickness on Physico-Chemical Properties of p-NiO (Bunsenite) Thin Films Prepared by the Chemical Spray Pyrolysis (CSP) Technique. *Optik (Stuttg).* **2016**, *127*, 1442–1449, doi:10.1016/j.ijleo.2015.11.026.

Preprints (www.preprints.org) | NOT PEER-REVIEWED | Posted: 7 September 2023 doi:10.20944/preprints202309.0442.v1

31. Taibi, M.; Ammar, S.; Jouini, N.; Fiévet, F.; Molinié, P.; Drillon, M. Layered Nickel Hydroxide Salts: Synthesis, Characterization and Magnetic Behaviour in Relation to the Basal Spacing. *J. Mater. Chem.* **2002**, *12*, 3238–3244, doi:10.1039/B204087E.
32. Andrade, T.M. de; Mariani, F.Q.; Nunes Júnior, C.V.; Dalpasquale, M.; Danczuk, M.; Anaissi, F.J. Compreendendo as Propriedades (Estrutural, Espectroscópica, Colorimétrica e Térmica) de Sais de Níquel. *Matéria (Rio Janeiro)* **2018**, *23*, doi:10.1590/s1517-707620170001.0312.
33. Qi, Y.; Qi, H.; Li, J.; Lu, C. Synthesis, Microstructures and UV–Vis Absorption Properties of β-Ni(OH)2 Nanoplates and NiO Nanostructures. *J. Cryst. Growth* **2008**, *310*, 4221–4225, doi:10.1016/j.jcrysgro.2008.06.047.
34. Gottardi, W.; Nagl, M. Chlorine Covers on Living Bacteria: The Initial Step in Antimicrobial Action of Active Chlorine Compounds. *J. Antimicrob. Chemother.* **2005**, *55*, 475–482, doi:10.1093/jac/dki054.
35. Brackett, R.E. Antimicrobial Effect of Chlorine on Listeria Monocytogenes. *J. Food Prot.* **1987**, *50*, 999–1004, doi:10.4315/0362-028X-50.12.999.
36. Bassioni, G.; Farid, R.; Mohamed, M.; Hammouda, R.M.; Kühn, F.E. Effect of Different Parameters on Caustic Magnesia Hydration and Magnesium Hydroxide Rheology: A Review. *Mater. Adv.* **2021**, *2*, 6519–6531, doi:10.1039/D0MA00887G.
37. Hao, L.; Zhu, C.; Mo, X.; Jiang, W.; Hu, Y.; Zhu, Y.; Chen, Z. Preparation and Characterization of Mg(OH) 2 Nanorods by Liquid–Solid Arc Discharge Technique. *Inorg. Chem. Commun.* **2003**, *6*, 229–232, doi:10.1016/S1387-7003(02)00725-6.
38. Kurt, H.I.; Ergul, E.; Yilmaz, N.F.; Oduncuoglu, M. Surface Functionalization of Nano MgO Particles with Nickel and Cobalt. *Mater. Res. Express* **2019**, *6*, 0850f1, doi:10.1088/2053-1591/ab278f.
39. Murtaza, M.; Aqib, A.I.; Khan, S.R.; Muneer, A.; Ali, M.M.; Waseem, A.; Zaheer, T.; Al-Keridis, L.A.; Alshammari, N.; Saeed, M. Sodium Alginate-Based MgO Nanoparticles Coupled Antibiotics as Safe and Effective Antimicrobial Candidates against Staphylococcus Aureus of Houbara Bustard Birds. *Biomedicines* **2023**, *11*, 1959, doi:10.3390/biomedicines11071959.
40. Liao, Y.-Y.; Pereira, J.; Huang, Z.; Fan, Q.; Santra, S.; White, J.C.; De La Torre-Roche, R.; Da Silva, S.; Vallad, G.E.; Freeman, J.H.; et al. Potential of Novel Magnesium Nanomaterials to Manage Bacterial Spot Disease of Tomato in Greenhouse and Field Conditions. *Plants* **2023**, *12*, 1832, doi:10.3390/plants12091832.
41. Nguyen, N.-Y.T.; Grelling, N.; Wetteland, C.L.; Rosario, R.; Liu, H. Antimicrobial Activities and Mechanisms of Magnesium Oxide Nanoparticles (NMgO) against Pathogenic Bacteria, Yeasts, and Biofilms. *Sci. Rep.* **2018**, *8*, 16260, doi:10.1038/s41598-018-34567-5.
42. Chaudhari, V.P.; Rajput, K.; Mondal Roy, S.; Chaudhuri, T.K.; Roy, D.R. Experimental and First-Principles Investigation on the Structural, Electronic and Antimicrobial Properties of Nickel Hydroxide Nanoparticles. *J. Phys. Chem. Solids* **2022**, *160*, 110367, doi:10.1016/j.jpcs.2021.110367.

Disclaimer/Publisher's Note: The statements, opinions and data contained in all publications are solely those of the individual author(s) and contributor(s) and not of MDPI and/or the editor(s). MDPI and/or the editor(s) disclaim responsibility for any injury to people or property resulting from any ideas, methods, instructions or products referred to in the content.